Spectral Characterization of the HIRDLS Flight Instrument From Prelaunch Calibration Data

Thomas Eden, Jr., John Barnett, John Gille, Karim Djotni, Chris Hepplewhite, Olusoji Oduleye, and John Whitney

***Abstract*—Results from an instrument-level spectral characterization of the 21-channel High Resolution Dynamics Limb Sounder (HIRDLS) flight instrument will be presented. These data were obtained during the prelaunch calibration of HIRDLS at the University of Oxford (fall 2002). A monochromator, equipped with a controllable diffraction grating, was used to produce monochromatic light for these tests. The monochromator was housed, along with HIRDLS, in a large vacuum chamber. The monochromator was also equipped with a polarizer, which allowed data to be acquired at known polarizations for each channel. A calibration detector, with a flat spectral response, was used to measure the output from the monochromator. This paper will document the analysis procedures used to obtain a measured instrument spectral response for each channel, along with the associated error analyses for these measurements.**

***Index Terms*—Diffraction grating, monochromator, polarization, spectral.**

I. Introduction

THE HIGH Resolution Dynamics Limb Sounder (HIRDLS) is a 21-channel infrared limb-scanning filter radiometer currently flying in orbit on the National Aeronautics and Space Administration (NASA) Earth Observing System Aura satellite. The conceptual design of HIRDLS was described in detail elsewhere [1]. The prelaunch calibration of the HIRDLS protoflight model occurred during fall 2002, at the University of Oxford, U.K. As part of this calibration exercise, an end-to-end instrument-level spectral calibration was performed. The HIRDLS instrument spectral response is primarily the product of the detector response and transmissions of several instrument components that make up the lens assembly, namely, the warm and cold band-defining interference filter assemblies, and the two germanium lenses located between the warm and cold filter assemblies. All reflective elements (i.e., scan mirror, primary and secondary mirrors, and folding mirror) in the optical chain contribute negligibly to any temperature-dependent spectral response shape change or losses in transmission. Prior to this prelaunch calibration, there were individual measurements and spectral responses calculated for each filter element set [2]; however, no subsystem measurements were ever performed.

The HIRDLS instrument was contained under vacuum, in a large vessel that was sizable enough to include calibration test equipment (TEQ) used to perform various tasks during the calibration exercise. For the spectral characterization of HIRDLS, a monochromator, equipped with a diffraction grating, was used to supply monochromatic light for these tests. The conceptual design and operation of the monochromator were also covered in a previous article [3].

For this end-to-end instrument spectral calibration, a conservative error budget was obtained for the measured instrument spectral responses derived from calculations of retrieval sensitivity to spectral response errors. The following error requirements were based on relative-response points (RRPs), where the response is a percentage of the peak response $(F_{\max})$.

1) Any relative spectral response measurement (defined as the ratio between the spectral response at a particular wavenumber and the maximum spectral response value for that channel and denoted in the text as $F(\overline{\nu})/F_{\max}$) between the 1% RRPs cannot have an error greater than 1.0%, with three samples per resolution element, at an absolute spectral accuracy of 0.2 cm^{-1} (one sigma).
2) The error in the relative spectral response between the 1% and 0.2% RRPs must not be greater than 100%.
3) Any detector spectral response measurements over the range of 400–2500 cm^{-1} (operating spectral range of the monochromator) and outside 0.2% RRPs are considered to be *out of band*. Here, any out-of-band response is considered to have its response greater than 0.1% of the peak in-band response $F_{\max}$, with a spectral resolution of 5% or better and a spectral accuracy of 10 cm^{-1}. This paper will not cover any results of the out-of-band measurements. However, what can be stated is that these out-of-band responses were very small and quite negligible. The dual-band interference filter arrays, implemented on the HIRDLS flight model, were designed specifically to greatly suppress out-of-band responses, which could impact the ability to retrieve data products at higher altitudes (low signal).

There were two main sources of temperature-dependent behavior that were characterized during the spectral calibration.

1) The relative response of the detectors will change depending on the detector focal-plane array (FPA) temperature.

Manuscript received May 11, 2009; revised November 23, 2009. Date of publication April 12, 2010; date of current version June 23, 2010. This work was supported in part by the National Aeronautics and Space Administration under Contract NAS5-97046, by the National Science Foundation through the National Center for Atmospheric Research, and by the Natural Environment Research Council in the U.K. under the High Resolution Dynamics Limb Sounder Project.

T. Eden Jr. is with National Center for Atmospheric Research, Boulder, CO 80307-3000 USA (e-mail: teden@ucar.edu).

J. Barnett, K. Djotni, C. Hepplewhite, and O. Oduleye are with the Department of Atmospheric, Oceanic, and Planetary Physics, University of Oxford, OX1 3PU Oxford, U.K. (e-mail: barnett@atm.ox.ac.uk; k.djotni@reading.ac.uk; hepplewhite@atm.ox.ac.uk; Olusoji.Oduleye@eumetsat.int).

J. Gille is with the University of Colorado at Boulder, Boulder, CO 80309 USA, and also with the National Center for Atmospheric Research, Boulder, CO 80307-3000 USA (e-mail: gille@ucar.edu).

J. Whitney, retired, was with the Department of Atmospheric, Oceanic, and Planetary Physics, University of Oxford, OX1 3PU Oxford, U.K. (e-mail: john.whitney@tiscali.co.uk).

Digital Object Identifier 10.1109/TGRS.2010.2043676

TABLE I
NOMINAL-OPERATING-CONDITION SPECTRAL CHARACTERISTICS FOR THE 21 HIRDLS CHANNELS. 50% RRP SPECTRAL BANDPASS RANGES AND WEIGHTED-MEAN WAVENUMBERS WERE DETERMINED FROM THIS PRELAUNCH INSTRUMENT SPECTRAL CALIBRATION EXERCISE

Channel Number	Principal Emitting Constituent	Spectral Bandpass (cm^{-1})	Weighted Mean Wavenumber (cm^{-1})
1	N_2O	566.87–584.29	575.09
2	CO_2	599.82–615.11	607.30
3	CO_2	612.06–636.52	623.84
4	CO_2	629.44–652.73	640.87
5	CO_2	657.09–680.81	668.85
6	Aerosols	819.89–834.94	827.26
7	$CFCl_3$	834.61–850.64	842.53
8	HNO_3	861.96–900.82	881.28
9	CF_2Cl_2	915.59–931.99	923.77
10	O_3	991.79–1008.49	1000.10
11	O_3	1013.70–1043.96	1028.75
12	O_3	1120.41–1139.69	1130.29
13	Aerosols	1202.61–1221.42	1212.10
14	N_2O_5	1230.47–1257.60	1243.86
15	N_2O	1255.93–1278.48	1267.43
16	$CLONO_2$	1279.19–1299.48	1289.32
17	CH_4	1327.04–1366.05	1346.38
18	H_2O	1386.95–1432.21	1409.37
19	Aerosols	1401.38–1415.50	1408.30
20	H_2O	1428.38–1532.57	1480.55
21	NO_2	1585.19–1632.92	1608.96

The cold filters are in direct thermal communication with the FPA; therefore, any increase in the FPA temperature during the life of the mission due to cryocooler degradation may cause changes in the spectral response shape for a given channel. Instrument-level spectral responses were obtained for all 21 channels at FPA temperatures of ∼61 K (nominal) and ∼71 K.

2) The warm spectral bandpass filter shapes are not expected to deviate significantly if thermostating drifts a few kelvin away from the controlled zonal heater temperature setting of 301 K. If thermostating of the warm-filter assembly and germanium lens #1 had degraded and was good only to, for example, 291 K, then the instrument spectral responses will need to be recharacterized; therefore, spectral response measurements were carried out at 291 K and $T_{\mathrm{FPA}} \simeq 61$ K.

Because of the limited time allocated for calibration, the number of off-nominal instrument spectral response measurements was concentrated mainly on the two conditions listed previously. Due to many factors, performing spectral measurements during calibration was very time consuming. A finer grid of measurements was originally envisaged over smaller off-nominal instrument temperature changes; however, what was accomplished has proven to be quite sufficient in characterizing the spectral performance of HIRDLS.

This paper will describe in detail how the HIRDLS in-band spectral response function was developed and obtained from the data analysis. Special consideration will be given to problems that were not anticipated during the data-analysis stage. Finally, a complete description of the statistical and systematic error analyses will conclude this paper. The principal emitting constituents, the 50% RRP spectral bandpass ranges, and the weighted-mean wavenumbers, as determined from this calibration exercise for each of the 21 HIRDLS channels, are shown in Table I.

II. DEFINITION OF A HIRDLS SPECTRAL RESPONSE

The basic definition of the HIRDLS spectral response as a function of wavenumber $F(\overline{\nu})$ can be written as

$$F(\overline{\nu}) = \frac{L_H(\overline{\nu})}{L_{\mathrm{IMR}}(\overline{\nu})}. \tag{1}$$

Here, L_H is the HIRDLS-detected channel radiance as a function of $\overline{\nu}$, and L_{IMR} is the incident flux of monochromatic radiance, emitted by the monochromator, as a function of $\overline{\nu}$.

A broadband hot source was used as the radiation source from which the monochromatic radiation was produced. Physically, the source was an electrical substrate cartridge type, manufactured by Heatwave, Inc., with a coated surface using molybdenum. The source could operate between ambient temperature and 1200 °C. The resulting monochromatic radiation that is incident on a detector had a typical bandwidth (defined by an exit slit) of 0.2–0.3 cm^{-1} and should fill the aperture-defining solid angle and detector field of view. This bandwidth determined the data-point spacing across the passband for each channel.

When viewing the monochromator exit slit, the impinging radiation was dispersed by the diffraction grating, along with emissions from other internal monochromator assembly surfaces. To monitor the monochromator background signal, a controllable shutter mechanism was used. The mechanism was located between the monochromator hot source and the entrance slit, just prior to the diffraction grating. With this device, views of the exit slit with *open* and *closed* states of the shutter were permitted, where the background signal levels were monitored with the shutter *closed* state. By taking the difference between these two shutter states at a given wavenumber setting, (1) can be rewritten as

$$F(\overline{\nu}) = \frac{\Delta L_H(\overline{\nu})}{\Delta L_{\mathrm{IMR}}(\overline{\nu})} \tag{2}$$

where $\Delta L_H(\overline{\nu}) = L_H^{\mathrm{open}}(\overline{\nu}) - L_H^{\mathrm{closed}}(\overline{\nu})$ and $\Delta L_{\mathrm{IMR}}(\overline{\nu}) = L_{\mathrm{IMR}}^{\mathrm{open}}(\overline{\nu}) - L_{\mathrm{IMR}}^{\mathrm{closed}}(\overline{\nu})$.

The radiation exiting the diffraction grating was polarized. An unpolarized HIRDLS spectral response was generated for each channel by taking data at two successive orthogonal polarization-step settings of the monochromator polarizer. For convenience, these settings are defined to be horizontal (h) and vertical (v), where, physically, the electric-field vector of the exiting radiation was aligned with the polarizer setting. The unpolarized HIRDLS response is then the sum of these two polarized responses

$$F(\overline{\nu}) = \frac{\Delta L_H^v(\overline{\nu})}{\Delta L_{\mathrm{IMR}}^v(\overline{\nu})} + \frac{\Delta L_H^h(\overline{\nu})}{\Delta L_{\mathrm{IMR}}^h(\overline{\nu})}. \tag{3}$$

The radiances shown in (1) are procured from digitized signal counts (S), with knowledge of detector gain (G). For any HIRDLS channel in question (for both v and h)

$$L_H(\overline{\nu}) = \frac{S_H(\overline{\nu})}{G_H} \tag{4}$$

and for the calibration detector used to monitor the flux of monochromatic radiance from the monochromator (neglecting

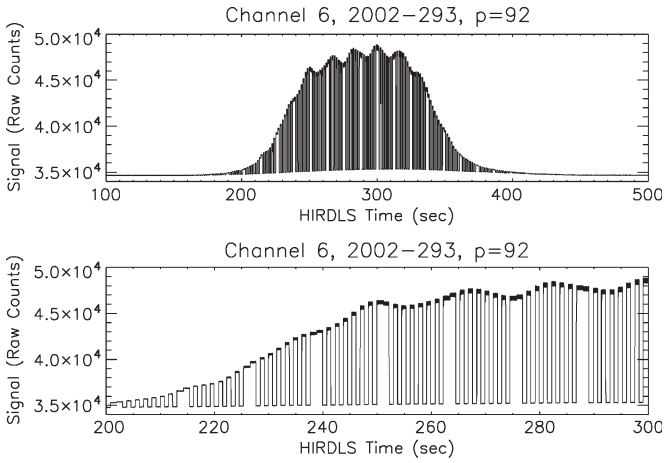

Fig. 1. Raw in-band spectral data for HIRDLS channel 6 at a polarization-step setting of $p = 92$ (vertical). (Top panel) Raw in-band response for the entire passband (i.e., between the 0.1% RRPs, which corresponds to a wavenumber passband of 808.5–846.6 cm^{-1}) in counts versus HIRDLS time. (Bottom panel) Exploded view of a smaller section of the top panel.

the polarization-step setting)

$$L_{\text{IMR}}(\overline{\nu}) = \frac{S_{\text{CD}}(\overline{\nu})}{G_{\text{CD}} F_{\text{CD}}(\overline{\nu})}. \tag{5}$$

Here, $F_{\text{CD}}(\overline{\nu})$ is the measured spectral response of the calibration detector. The calibration detector gain G_{CD} has a commanded gain setting depending on the passband and polarization-step setting. The HIRDLS detector gain G_H is obtained from an instrument radiometric calibration. Equation (3) can now be rewritten as

$$F(\overline{\nu}) = F_{\text{CD}}(\overline{\nu}) \left(\frac{\Delta S_H^v(\overline{\nu}) G_{\text{CD}}^v}{\Delta S_{\text{CD}}^v(\overline{\nu}) G_H^v} + \frac{\Delta S_H^h(\overline{\nu}) G_{\text{CD}}^h}{\Delta S_{\text{CD}}^h(\overline{\nu}) G_H^h} \right). \tag{6}$$

Note that $G_H^v = G_H^h$ and is not a commandable-type gain, which could very well be omitted from this derivation, but remains for the sake of completeness.

Although there were no specific requirements, the two terms on the right-hand side of (6) should contribute equally to $F(\overline{\nu})$. There will be more on this topic in Section IV-C.

III. Experimental Conditions and Data Acquisition

A. HIRDLS In-Band Spectral Responses

A raw in-band spectral data sample for HIRDLS channel 6 is shown in Fig. 1. These data were obtained under nominal FPA and lens #1 operating conditions, i.e., $T_{\text{FPA}} \simeq 61$ K and $T_{\text{Lens1}} \simeq 301$ K, respectively. The top panel displays the raw response over the entire passband in counts against HIRDLS time, which used an appropriate order-sorting (OS) filter, for a vertical polarization-step setting ($p = 92$; the horizontal polarization-step setting was $p = 36$). Note that these polarization-setting values have no physical significance, denoting only horizontal or vertical polarizer angle settings. The data-acquisition rate was 500 Hz, which yielded a data bandwidth acceptance of one selected detector response in the data stream. An exploded view of a portion of the data pattern is shown in the bottom panel. The in-band response changes in time due to two different mechanisms: monochromator shutter movement and grating position change. The shutter movements and grating position steps were controlled by an external computer that was synchronized to an 83-Hz clock from HIRDLS. The periodic pattern was generated by control commands contained in an input-command matrix executed on the external computer, where prescribed incremental grating position steps occurred during shutter-closed and "big-toothed" shutter-open events. Data were acquired between the 0.1% RRPs, at a resolution between 0.2 and 0.3 cm^{-1} for all channels. The in-band spectral response and its associated total error (statistical and systematic) were reported and used for each channel between the 0.2% RRPs.

Most of the HIRDLS-polarized in-band spectral response data (including the data run shown in Fig. 1) were acquired with the use of an optical OS filter, which was located after the diffraction grating and before the monochromator entrance slit. These filters rejected higher ordered diffracted photons of order λ/n, where $n = 2, \ldots, \infty$. Data were also taken without the OS filter in place and were important in verifying TEQ artifacts that appeared in the HIRDLS in-band responses.

An important set of HIRDLS in-band spectral response data was obtained using a filled gas cell, also located after the diffraction grating. These data were useful in verifying the transformation algorithm for putting the HIRDLS in-band response onto a wavenumber grid. Locations of known discernible absorption features in the HIRDLS in-band response were compared to laboratory data for a given gas cell. More details will be given in Section IV.

Prior to calibration, the manufacturer of the monochromator (Bentham, Ltd.) calibrated the sine drive (grating rotation angle against step motor movement) with a He–Ne laser positioned along the principal axis of the monochromator. Reported errors at the three-sigma level were less than 0.1 cm^{-1} and typically 0.02 cm^{-1}.

B. Monochromator Calibration Detector Responses

A similar data-taking procedure was utilized to monitor the output of the monochromator. A triglycine sulfide (TGS) thermistor bolometer detector was employed for this task and was physically located outside of the monochromator with a view of the exit slit by way of a flip mirror. For each polarization setting and selected OS filter, data were acquired over the same passband range as that of its HIRDLS in-band response counterpart. The resolution of the TGS calibration detector response over the measured passband range was more coarsely gridded than its HIRDLS counterpart because fine-structured behavior from the monochromator was not a concern. Monochromator shutter and grating-step movements were controlled by an external computer with a command-input matrix, which is similar to that used in obtaining HIRDLS spectral response data.

Prior to calibration, the same monochromator TGS calibration detector went through a spectral measurement over the HIRDLS spectral range of 6–18 μm. The measurements were performed at the National Physical Laboratory (NPL) in England. A plot of the measured spectral response of the monochromator calibration detector from the NPL calibration is shown in Fig. 2. The filtered response (solid red line) was obtained by applying a low-pass filter to the data. This filtered

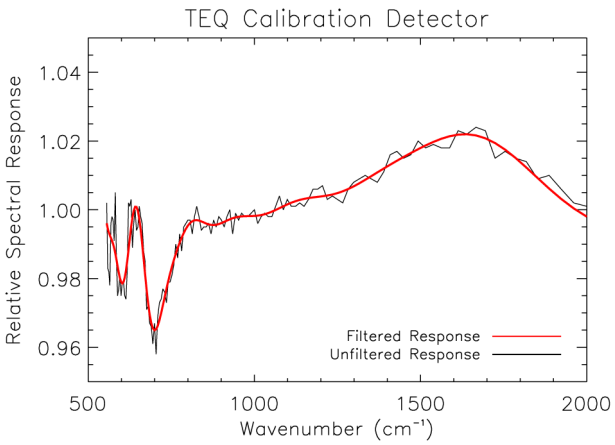

Fig. 2. Monochromator calibration detector spectral response (in relative-response units against wavenumber).

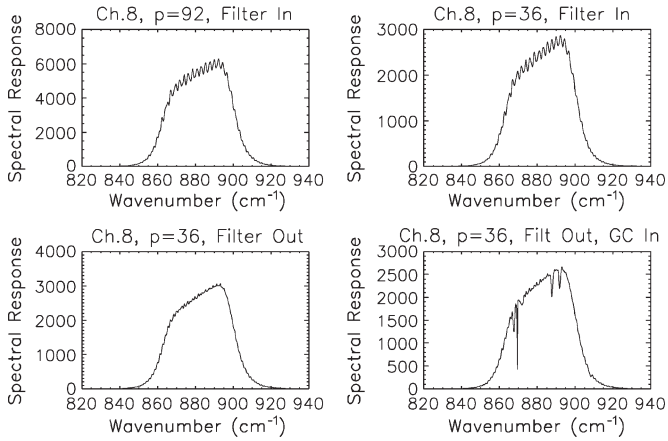

Fig. 3. Results from the Step-1 analyses of raw in-band spectral responses (in counts against wavenumber) for HIRDLS channel 8. (Top left) Spectral response with an OS filter at $p = 92$. (Top right) Spectral response with an OS filter at $p = 36$. (Bottom left) Spectral response without an OS filter at $p = 36$. (Bottom right) Spectral response with an NH_3 gas cell and without using the OS filter, at $p = 36$.

response (F_{CD}) was used in the eventual data analysis to obtain the final unpolarized responses.

C. Experimental Conditions

Spectral data were acquired at the following three different experimental conditions.

1) Nominal in-orbit operating conditions: $T_{\mathrm{FPA}} \simeq 61$ K and $T_{\mathrm{Lens1}} = 301$ K.
2) Off-nominal test #1 conditions: $T_{\mathrm{FPA}} \simeq 71$ K and $T_{\mathrm{Lens1}} = 301$ K. The intent here was to examine any channel-dependent spectral response behavior for a 10-K increase in the FPA temperature.
3) Off-nominal test #2 conditions: $T_{\mathrm{FPA}} \simeq 61$ K and $T_{\mathrm{Lens1}} = 291$ K. This test was initiated to examine any channel-dependent spectral response changes due to a decrease in the lens #1 temperature and corresponding cooling of the warm-filter assembly.

The time and effort required to implement these tests were extensive. If conditions in orbit strayed away from the nominal FPA and lens #1 temperature settings, the appropriate off-nominal-condition data would be used to adjust our spectral responses, channel by channel. However, for most channels, the spectral response shapes were invariant to these thermal changes.

IV. Data Analysis

The first step in analyzing the raw in-band spectral responses was to perform a difference analysis (shutter open minus shutter closed) as a function of the diffraction grating position. An important detail to this analysis was being able to map the externally controlled input-matrix commands onto HIRDLS time. Even though the matrix input was synchronized to the 83-Hz clock of HIRDLS, absolute knowledge of where the command matrix starts and where all movements of the monochromator shutter and diffraction grating mechanisms occur in HIRDLS time was essential for performing this phase of the analysis, which will be called *Step 1*. Additional information needed by the analysis software was extracted from the Science Algorithm Implementation Language diagnostic block, which was located in the HIRDLS science data stream. This datum, which was recorded at a rate of 1.3 Hz, contained important information concerning the experimental conditions of the monochromator during a given data-acquisition run.

For each grating position, a statistical mean was calculated for each state of the shutter, and a resulting difference was computed. Finally, the grating position was then converted into wavenumber. The results from a series of in-band spectral runs for HIRDLS channel 8 (HNO_3 channel) are shown in Fig. 3. The top two panels in Fig. 3 show data runs using an appropriate OS filter at the two intended orthogonal polarization settings. In each spectral response, there are high-frequency periodic wave structures spanning most of the passband. These structures emanated from the TEQ, namely, reflections from the OS filter substrate surfaces. The next analysis step dealt with the removal of these artifacts from the HIRDLS spectral response (see the next section for details). The bottom left panel in Fig. 3 shows a data run where an OS filter substrate was not used. Notice the existence of the low-amplitude high-frequency structures in this spectrum. Because the OS filter was not used, these structures are attributed to surface reflections from the polarizer; accordingly, these structures must also be identified and removed. Finally, the lower right panel in Fig. 3 shows a data run using an NH_3 gas cell. The spectral response exhibits discernible absorption features that can be compared to known laboratory transmission spectra. The detected and predicted absorption peak locations for channel 8 are shown in Table II. All detected peak locations in Table II agree with the corresponding predicted laboratory absorption peak locations to within the data resolution of the measurement, which was nominally 0.25 cm^{-1}. These results verify the method employed for transforming the spectral response onto a wavenumber grid. Further reinforcement of the accuracy of this technique was observed in the analyses of other channels that had gas-cell runs with recognizable absorption features.

A. Step 2: Removal of TEQ-Induced Spectra

Because we are seeking an unpolarized HIRDLS in-band spectral response for each channel, the periodic wave structures, as seen in Fig. 3, must be removed from the "true" HIRDLS

TABLE II
DETECTED ABSORPTION PEAK LOCATIONS IN THE CHANNEL-8 SPECTRAL RESPONSE, AS SHOWN IN THE BOTTOM RIGHT PANEL IN FIG. 3. THESE VALUES ARE COMPARED TO KNOWN LOCATIONS OBTAINED FROM LABORATORY TRANSMISSION SPECTRA. THE LAST COLUMN IS A DIFFERENCE BETWEEN THE TWO VALUES. ALL VALUES ARE WITHIN THE NOMINAL DATA RESOLUTION OF 0.25 cm^{-1}

Detected Location (cm^{-1})	Predicted Location (cm^{-1})	Offset (cm^{-1})
867.7	867.5	0.2
872.3	872.1	0.2
887.8	887.6	0.2
891.9	891.8	0.1

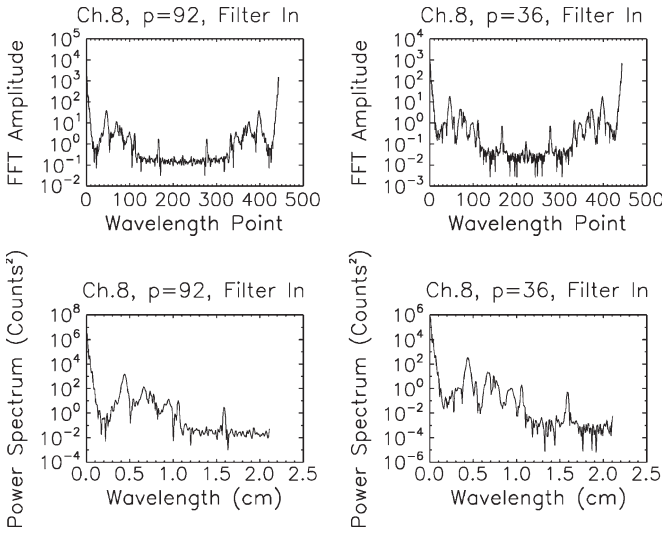

Fig. 4. Step-2 analyses of the in-band spectral responses for HIRDLS channel 8. (Top left) Fourier transform of the channel-8 spectral response (counts against wavelength point), with an OS filter, for $p = 36$. (Top right) Fourier transform of the channel-8 spectral response (counts against wavelength point), with an OS filter, for $p = 92$. (Bottom left) Power spectrum of the top left FFT spectrum ($counts^2$ against wavelength). (Bottom right) Power spectrum of the top right FFT spectrum ($counts^2$ against wavelength point). In the bottom plots, the peak centered at ∼0.45 cm represents the wavelength that contributes mostly to the periodic features observed in the channel-8 responses in the top panels in Fig. 3.

spectral response line shape. As discussed earlier in Section IV, these high-frequency features are artifacts of the TEQ, i.e., the OS filter and the polarizer. The following two techniques were tested to eradicate these spectra:

1) frequency-domain fast Fourier transform (FFT) filtering;
2) modulated sinusoidal wave fitting.

For this application, the FFT filtering scheme had been employed for these analyses and will be described here.

Owing to the fact that the TEQ spectra were periodic in the wavenumber space, the FFT filtering method seemed to be a logical choice for understanding these spectra and their effective removal. Indeed, if an FFT was performed on these spectral responses, these TEQ spectra should be readily identifiable. This idea is confirmed in Fig. 4. The top two panels in Fig. 4 show the results of performing an FFT on both polarized responses for channel 8. Note that the absolute value of the complex Fourier coefficients is plotted in the wavelength domain. What is immediately noticeable about these results are the structures located between the 20 and 120 wavelength points. These peaks represent where the TEQ spectra reside in the wavelength-point space. In particular, the peak at ∼45 wavelength points is produced by the OS filter. This notion can be substantiated by fitting a modulated sinusoidal wave to these spectra in the Step-1 spectral responses. Results from the fits to the channel-8 polarized spectral responses revealed that the fitted angular parameter was ∼0.45 cm, which is also observed in the power spectra as a function of wavelength (see bottom panels in Fig. 4). All other relevant structures at higher wavelength-point numbers, up to the Nyquist partition, originate mostly from the polarizer.

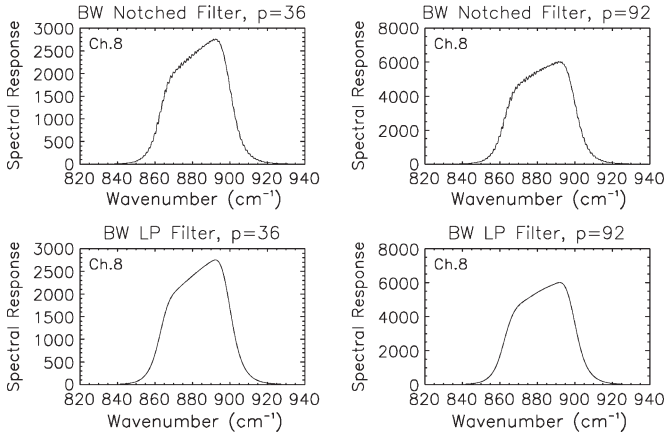

Fig. 5. Step-2-polarized FFT-filtered spectral responses (counts against wavenumber) for HIRDLS channel 8. (Top panels) FFT-filtered spectral responses using an appropriate band-reject filter (as described in the text) to remove *only* those wavelength points correlated with the contributions from the OS filter. (Bottom panels) FFT-filtered spectral responses using a band-reject filter. These polarized HIRDLS responses will be used to assemble the unpolarized responses.

By using an appropriate filter on these FFT spectra, all unwanted higher wavelength structures are effectively removed from the basic spectral response line shape. In this analysis, a high-order Butterworth low-pass filter was used to perform this exercise. The mathematical form of the low-pass filter function $f_{\rm lp}$ is given by

$$f_{\rm lp}(x) = [1 + (x/\lambda_{\rm cut})^n]^{-1}. \tag{7}$$

Here, x is the wavelength point, $\lambda_{\rm cut}$ is the cutoff wavelength point, and n is the filter order. The results presented here used $n = 16$ in (7) for all channels. To remove the wavelength components emanating only from the OS filter, a band-reject or notched filter was devised. This notched filter was produced from a high-pass Butterworth filter [i.e., $f_{\rm hp}(x) = 1 - f_{\rm lp}(x)$] and summed together with (7). The results are shown in Fig. 5. The top panels in Fig. 5 demonstrate the effectiveness of using this band-reject filter in removing only the OS filter contribution to the spectral responses. Note the similarity of the $p = 36$ spectral response (top left panel) to the one shown in the bottom left panel in Fig. 3. The bottom panels in Fig. 5 show the spectral responses with all TEQ artifacts removed using (7). These polarized responses are now ready to be used to obtain the unpolarized spectral response.

B. Removal of Detector Nonlinearities

It is appropriate, at this time, to mention the process of removing detector nonlinearity from the spectral response profiles. The 21 mercury-cadmium-telluride photoconductive

detector elements employed on HIRDLS exhibit varying degrees of nonlinearity for large incident radiance signals, where the amount of nonlinearity present in each channel was determined from prelaunch radiometric calibration data [4].

Because the atmospheric radiance impinging on a HIRDLS detector should produce a linear response through its saturation point, it was necessary to remove any detector nonlinearity from a signal produced by the HIRDLS instrument. Consequently, relevant calibration data products, such as detector spectral responses, should undergo this removal process, which could affect a spectral response shape.

A raw signal (S) from a HIRDLS detector can be represented in terms of a detected radiance signal (L), with knowledge of the detector gain (G), and a second-order term for nonlinearity (k)

$$S = GL(1 + kL). \tag{8}$$

The aforementioned relationship is inverse to what is done in orbit, where a HIRDLS signal in counts is converted into a radiance. At a more basic level, the main difference is that there is no space-view signal in (8). The reason here is due to the fact that the scan mirror is staring at the HIRDLS channel (no staring at a cold reference target), and a difference between monochromator open and closed states was sought. With the focal plane cooled to the same temperature as the radiometric calibration, along with the filters, lens assemblies, and other optical elements controlled to identical temperatures, G and k in (8) can be used with confidence in this nonlinearity removal analysis.

Using instrument-calibrated k and G for each channel, a HIRDLS-detected radiance signal can be deduced

$$L = -\frac{1}{2k} \pm \frac{1}{2}\left[\frac{1}{k^2} + \frac{4S}{kG}\right]^{1/2}. \tag{9}$$

The root used from (9) depends on the sign of k. If k is positive (negative), then the positive (negative) root is retained. To procure the equivalent linear signal S_{corr} from a particular L, the term with G is used alone in (8)

$$S_{\text{corr}} = GL. \tag{10}$$

This method was applied on the raw data, where the procedure removed the nonlinear contribution from each recorded digitized signal (both shutter-open and shutter-closed signals). The nonlinearity-removed spectral responses (red line) for channels 1, 2, 13, and 21 using the $p = 36$ (horizontal) polarization-step setting are shown in Fig. 6. The spectral responses with the nonlinearity removal algorithm turned off are also shown in the same plots. The strength of the nonlinearity removal procedure varies noticeably between channels. Because of the small value for k in channel 1, both responses are nearly identical. The increased effect from the nonlinearity removal procedure in channel 2 results mostly from large radiometric signals (above 60-K counts) for the monochromator shutter-open states. For channel 13, the effect of the nonlinearity removal procedure is augmented mostly by the size of k. Here, moderate signals will be enhanced because of the larger value of k.

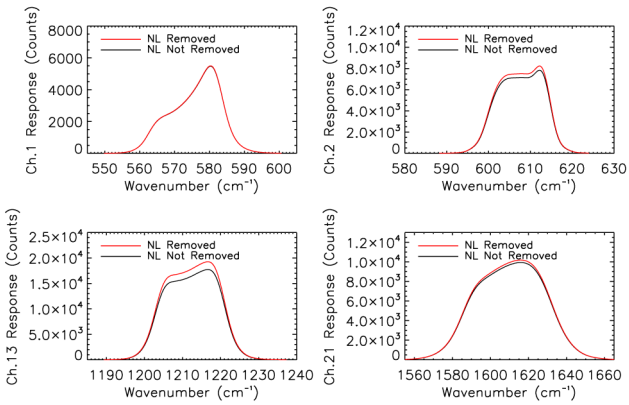

Fig. 6. Spectral responses (counts against wavenumber) for channels 1, 2, 13, and 21, at a polarization setting of $p = 36$. Note that these responses have not been ratioed with their associated monochromator output spectrum.

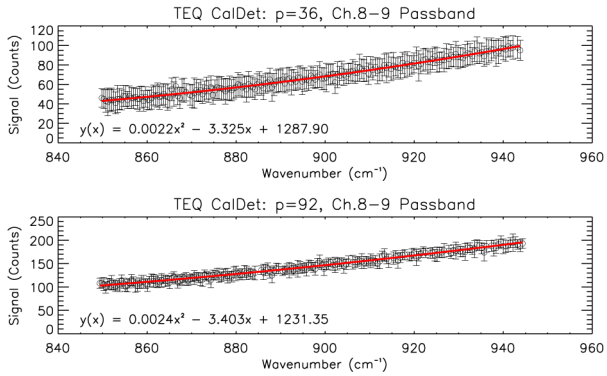

Fig. 7. Calibration detector responses with one-sigma error bars, for the passband of channels 8–9, in counts against wavenumber. As with the HIRDLS spectral responses, these data included the OS filter. The (red line) equation for each quadratic fit is also shown. (Top panel) Analyzed calibration detector response for $p = 36$. (Bottom panel) Analyzed calibration detector response for $p = 92$.

C. Step 3: Polarization Differences and Unpolarized Spectral Responses

The next analysis step involves the polarized spectral responses shown in the bottom panel in Fig. 5. These responses must be ratioed with their corresponding polarized calibration detector responses. The monitoring of the monochromator output is essential for obtaining a correct HIRDLS response for each polarization setting. These data were generally obtained at times prior to, or just after, the associated HIRDLS spectral data runs were performed. Barring a few exceptions, the responses of the calibration detector were slowly varying and of a simple shape for all channels. The analyzed calibration detector responses for the bandpass of channels 8–9, at each polarization setting, are shown in Fig. 7.

The analysis of these data was quite similar to the Step-1 analysis for the HIRDLS spectral responses (see Section IV); accordingly, a difference analysis between the monochromator shutter-open and shutter-closed states was performed for each diffraction grating setting, and then, the response was placed onto a wavenumber grid. The solid red line represents the best least squares fit of a second-order polynomial function to the data. The one-sigma errors were used to weigh each data point in the fit. The equation for the fit is displayed on each panel in Fig. 7.

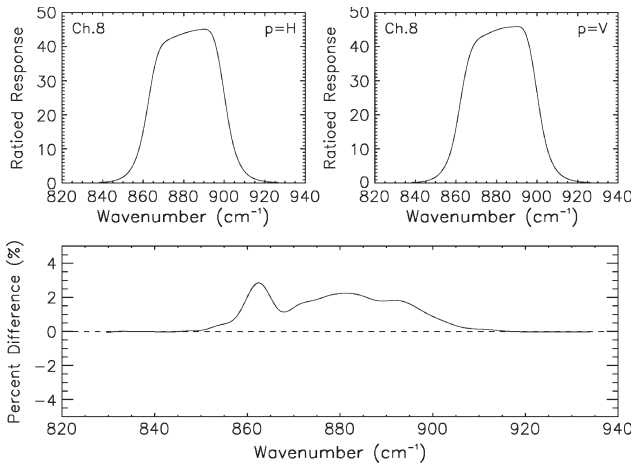

Fig. 8. Polarization differences of ratioed spectral responses for HIRDLS channel 8. (Top plots) Ratioed spectral responses (against wavenumber) for each polarization setting. (Bottom plot) Percent difference between the aforementioned polarized responses as a function of wavenumber.

Although the data are noisy in Fig. 7, the spectrum was structureless, which was anticipated. The fit residual errors were treated accordingly in the final error analysis, which will be presented in Section V.

The polarized spectral responses are now ready to be ratioed with their respective calibration detector responses. Although there were no accuracy requirements for the polarization difference for a given channel, the difference between each ratioed polarized HIRDLS spectral response should be small. The difference in polarization was computed using the following relation:

$$\Delta F(\overline{\nu}) = \frac{F_{p=92}(\overline{\nu}) - F_{p=36}(\overline{\nu})}{F^{\max}_{p=36}(\overline{\nu})}. \tag{11}$$

The results for channel 8 are shown in Fig. 8. For these particular channel-8 data runs, the calibration detector gains for each polarization setting were identical, i.e., $G^{v}_{\mathrm{CD}} = G^{h}_{\mathrm{CD}} = 1$. The two polarized spectral responses in Fig. 8 can now be summed together to obtain the unpolarized spectral response for channel 8. The peak-normalized unpolarized spectral responses for channel 8, from the three data sets acquired during calibration, are shown in Fig. 9. The results for the four temperature-sounding CO_2 HIRDLS channels, following the same analysis procedures as described in the text, are shown in Fig. 10. In this set of plots, spectral responses from the two off-nominal-experimental-condition data are also included. The slight spectral shift on the high wavenumber side in channel 4 is due solely to the mismatch between the warm and cold filter passbands at 71 K.

V. Error Analysis

Each HIRDLS instrument spectral response is composed of many measurements at incremental wavenumber settings throughout an entire passband. The monochromator output spectrum is collected in a similar manner. By and large, the nature of these measurements requires that, for a given error component, an error distribution over the passband be calculated, regardless of whether the error under investigation is statistical (random) or systematic to the measurement.

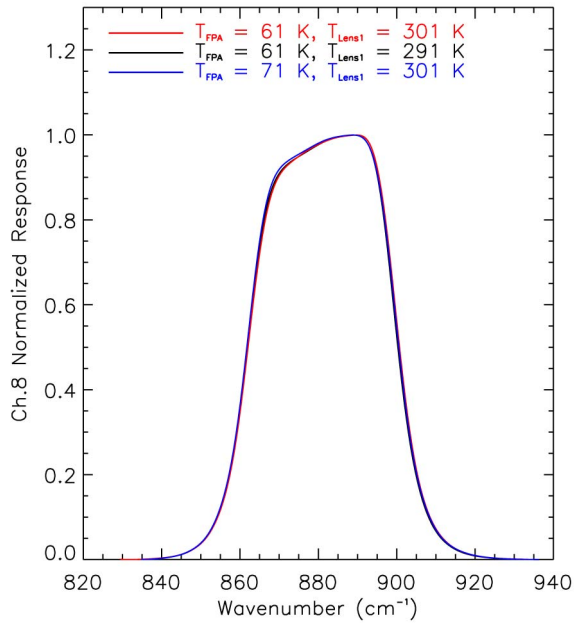

Fig. 9. Fully analyzed unpolarized HIRDLS spectral responses for channel 8, in peak-normalized units against wavenumber.

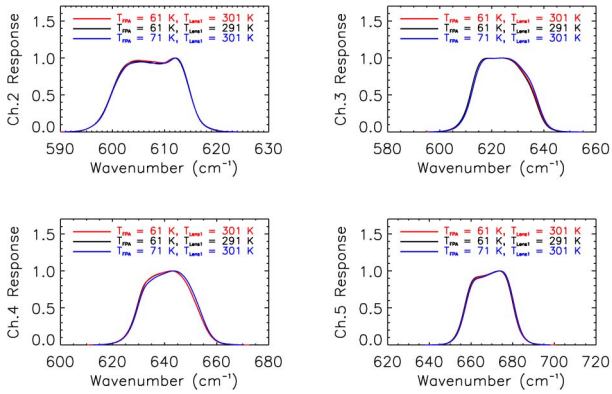

Fig. 10. Fully analyzed unpolarized HIRDLS spectral responses (in peak-normalized units against wavenumber) for channels 2–5 (temperature-sounding CO_2 channels).

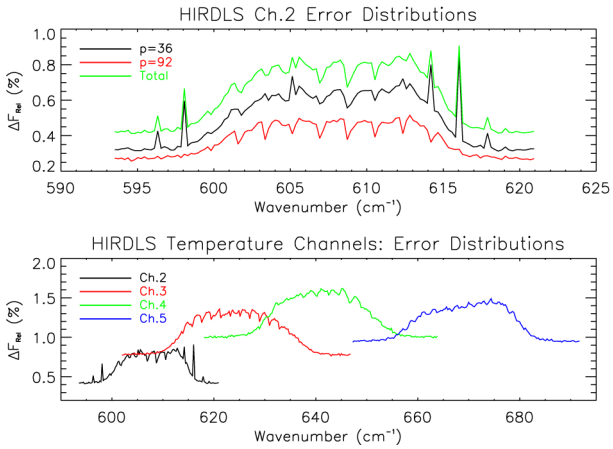

Fig. 11. Statistical uncertainty distributions $\Delta F_{\mathrm{rel}}(\overline{\nu})$ (in percent), for the HIRDLS spectral response measurements, plotted against wavenumber. (Top panel) Channel-2 spectral response error distributions for the two measured polarization-step settings, along with the quadrature-summed total. (Bottom panel) Quadrature-summed error distributions for all four temperature-sounding (CO_2) channels.

Statistical and systematic error contributions will be discussed in the following in separate sections.

A. Statistical Errors

1) HIRDLS Response: Sources for statistical error emanate mainly from computing the mean signal difference between shutter-open and shutter-closed cases for both $\Delta L_H(\overline{\nu})$ and $\Delta L_{\mathrm{IMR}}(\overline{\nu})$, as a function of $\overline{\nu}$. The main difference between these two quantities is that the error distribution for $\Delta L_{\mathrm{IMR}}(\overline{\nu})$ is used to weigh the fit in the monochromator output spectrum (see Fig. 7 and Section IV-C).

For each HIRDLS spectral response, an error distribution spectrum for $F_{\mathrm{rel}} = F(\overline{\nu})/F_{\max}$ at each polarization setting is computed. Propagating the errors in this expression yields the following relationship:

$$\Delta F_{\mathrm{rel}}(\overline{\nu}) = F_{\mathrm{rel}}(\overline{\nu}) \left[\left(\frac{\Delta F(\overline{\nu})}{F(\overline{\nu})} \right)^2 + \left(\frac{\Delta F_{\max}}{F_{\max}} \right)^2 \right]^{1/2}. \quad (12)$$

Indication of polarization-setting dependence is suppressed here for simplicity. The total error from both polarization settings is now obtained in the usual way

$$\Delta F_{\mathrm{rel}}(\overline{\nu}) = \left\{ \left[\Delta F^h_{\mathrm{rel}}(\overline{\nu}) \right]^2 + \left[\Delta F^v_{\mathrm{rel}}(\overline{\nu}) \right]^2 \right\}^{1/2}. \quad (13)$$

The HIRDLS statistical error distributions $\Delta F_{\mathrm{rel}}(\overline{\nu})$ for the CO_2 channels plotted against wavenumber are shown in Fig. 11. The top panel displays the channel-2 statistical error distributions for both polarization-step settings (i.e., $p = 36$ and $p = 92$) and the quadrature-summed total. The outlying spikes are due to signal fluctuations because of an intermittent ringing shutter mechanism, when the shutter went from closed to open, causing a larger-than-expected sample standard deviation for that measurement. The bottom panel displays the quadrature-summed total error for the four CO_2 channels. These distributions are shown between the 0.1% RRPs.

It is worth noting at this point that $\Delta F_{\mathrm{rel}}(\overline{\nu})$ represents the largest component of the overall error, both statistically and systematically. For some channels, this error alone is greater than the HIRDLS Instrument Requirements Document specification between the 1% RRPs.

The main factor contributing to this outcome is that, during episodes of large detected fluxes (i.e., near the middle of the spectral response), large statistical fluctuations are observed for a given wavenumber setting. A clear demonstration of this phenomenon is observed in Fig. 1 (bottom panel). In general, albeit with a few exceptions, for shutter-open conditions, as the detected flux increases, the size of the standard deviation about the mean detected signal increases.

Before any measurements were taken, emitted monochromator fluxes impinging on a HIRDLS detector were estimated based on instrument throughput and detector sensitivity. For some channels, there is a large polarization-setting dependence. The emitted flux impinging on a HIRDLS detector can be controlled either by adjusting the entrance or exit slit widths in the monochromator or by adjusting the broadband hot source. For the most part, to obtain reasonable detector output signals through the entire passband, the former method was used to alter the amount of emitted flux when the initial estimated monochromator settings were not adequate.

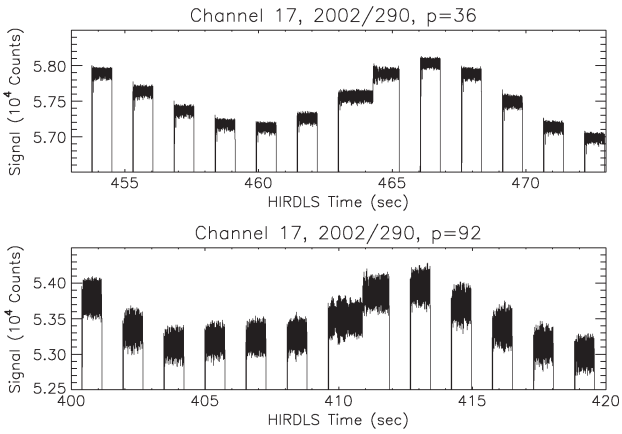

Fig. 12. Close-up of channel-17 raw shutter-open signals (in 10^4 counts against HIRDLS time) for both the (top panel) $p = 36$ and (bottom panel) $p = 92$ polarization settings, where the spectral response passband regions are nearly equal for both data sets. To further bring out a direct comparison of the noise levels between each polarization setting, both panels have identical ordinate scale ranges.

One instance that disagrees with this general description is the nominal-condition spectral response measurements for channel 17. The slit widths were adjusted separately to create detected responses that are similar in magnitude for each polarization setting; however, the $p = 92$ response, which had an overall smaller magnitude through the passband compared to its $p = 36$ counterpart, had a much larger standard deviation through the most spectrally sensitive wavenumbers. These results are shown graphically in Fig. 12.

2) Calibration Detector: The remaining statistical components to the overall HIRDLS spectral response error originate from the calibration detector monochromator output spectra for each polarization measurement, along with the spectral response measurement for this detector. With respect to the analysis flow, this error component was calculated after the HIRDLS spectral response had been transformed onto a wavenumber grid and FFT filtered. The ratioed spectral responses are recalculated, where the calibration detector output spectra are adjusted by the root-mean-square deviation of fit residuals $\pm\delta_{\mathrm{rms}}$, and a percent difference is computed against the central ratioed response shape.

To compute δ_{rms}, the monochromator output spectra for each polarization setting must be used. The error bars shown in Fig. 7 were quadrature-summed error levels for both shutter-open and shutter-closed positions computed at a given diffraction grating position setting and were eventually translated onto a wavenumber grid. Recall that the wavenumber grid utilized for the calibration detector response was more coarse than its HIRDLS counterpart. For all channels and polarizations, except channel 5 at the $p = 92$ setting (Wood's anomaly [6]), the calibration detector responses were often simple and smoothly varying shapes over a respective passband that could be theoretically represented by a low-order polynomial function. A function minimization procedure [5] was used to perform the fit, where the errors were used to weigh the function being minimized. δ_{rms} was then computed from the sum of fit residuals.

Results will be shown in a plot with the remaining contributions to the overall $\Delta F_{\rm rel}(\overline{\nu})$ at the end of Section VI.

3) Calibration Detector Spectral Response: The smallest statistical error component to $\Delta F_{\rm rel}(\overline{\nu})$ resulted from the uncertainty in the calibration detector spectral response. To calculate $\delta_{\rm rms}$ for the calibration detector spectral response, the filtered response [see Fig. 2 (solid red line)], which was used to compute the HIRDLS spectral response shapes, was differenced with the actual data points (solid black lines). The ratioed HIRDLS spectral response was then recalculated with $F_{\rm CD} \pm \delta_{\rm rms}$ and compared to the central HIRDLS spectral response (using only $F_{\rm CD}$), where a percent difference distribution was then calculated.

B. Systematic Errors

Systematic errors fall into the following three distinct and analyzable categories:

1) change in spectral response due to removing detector nonlinearity from the detected signal;
2) change in spectral response due to the cutoff wavelength location when removing TEQ-induced structures;
3) change in spectral response due to hot-source temperature stability. Because of time constraints, this error component was only investigated for channel 1, which is radiometrically the noisiest channel of the 21 HIRDLS channels. After realizing the resulting error distribution to be sufficiently small for channel 1, further measurements on other channels were deemed unnecessary.

Details for each of these items follow.

1) Removing Detector Nonlinearity: Removing detector nonlinearity from the HIRDLS spectral response data requires knowledge of the detector nonlinearity constant k. This factor is obtained from an associated instrument radiometric calibration and is described elsewhere in this issue [4] The uncertainty in determining k can then be used to understand its influence on the spectral response line shape and its systematic contribution to $\Delta F_{\rm rel}(\overline{\nu})$.

Determining the error in removing detector nonlinearity from the raw signal was carried out by propagating the errors in (9)

$$\Delta L = \Delta S \frac{\partial L}{\partial S} + \Delta k \frac{\partial L}{\partial k} + \Delta G \frac{\partial L}{\partial G} \tag{14}$$

where ΔS, Δk, and ΔG were all procured from the associated prelaunch instrument radiometric calibration [4]. With knowledge of ΔL, the error in the corrected signal can be obtained

$$\Delta S_{\rm corr} = S_{\rm corr} \left[\left(\frac{\Delta G}{G} \right)^2 + \left(\frac{\Delta L}{L} \right)^2 \right]^{1/2}. \tag{15}$$

Once $\Delta S_{\rm corr}$ is produced, new spectral response line shapes are generated from $S_{\rm corr} \pm \Delta S_{\rm corr}$ and are then compared to the spectral response line shape from $S_{\rm corr}$ alone, where an error distribution over the passband is produced.

2) FFT Filter Cutoff Wavelength: The cutoff wavelength point used in the low-pass filtering of channel 8 (Fig. 4, both polarization settings) is 14. Applying the filter removes all TEQ-induced structures, leaving behind the true spectral response line shape of the warm–cold filter combination. To examine the systematic error in using this cutoff wavelength point, new spectral response line shapes were calculated for 14 ± 1 wavelength points. These new response line shapes were then compared to the response line shape calculated using the central filter cutoff wavelength point, and finally, a percent difference distribution is then computed.

3) Flux Stability of Hot-Source Assembly: The hot-source assembly was a potential source for systematic error. In particular, its location to certain structures, such as the entrance slit and shutter, could cause conductive heating of these structures and alter the radiation environment in the monochromator. Cold shielding was designed to enclose the assembly to minimize the conductive heating of these structures. Nevertheless, it was necessary to estimate its contribution to the overall systematic error.

As was stated earlier, it was determined that the error contribution was inconsequential for channel 1 (noisiest channel), thereby nullifying any further measurement efforts on the other 20 channels.

VI. Conclusion

A detailed account of the analysis procedures used to obtain measured instrument spectral responses for all 21 channels from a prelaunch calibration of HIRDLS has been presented. Three different data sets, based on three realistically different instrument conditions, were analyzed. The results show that the spectral response line shapes between the three different data sets are quite similar, with only minor variations present. If the in-orbit conditions of the instrument change, e.g., warming of the FPA, then the spectral responses used to calculate forward-model transmittance tables may need to be adjusted accordingly.

Translating the measured instrument spectral response from HIRDLS time into the wavenumber space was very accurate and compared quite well with laboratory absorption spectra. All channels with sharp discernible absorption peaks were within the nominal spectral resolution ($\sim$0.25 cm^{-1}) of the measurement.

Unanticipated problems encountered in the HIRDLS spectral response measurements, e.g., of reflections emanating from the monochromator OS filter and polarizer surfaces, were effectively eradicated from the true spectral response line shape by using frequency-domain FFT filtering methods. After Fourier transforming the raw spectral responses, these unwanted spectral features were clearly separated from the true spectral response line shape, making low-pass filtering a sound method for removing these features.

The calibration detector provided ample snapshots of the monochromator output. These data runs immediately preceded or followed a HIRDLS spectral response measurement. Except for the $p = 92$ setting for channel 5 (due to Wood's anomaly [6], which is a rapid variation in the amplitudes of the diffracted spectral orders, corresponding to an onset or disappearance of a particular spectral order), all monochromator output spectra were smoothly varying but quite noisy. The output spectra could be fit with low-order polynomials (most through order two, except channels 3 and 4, which required an order-four polynomial for the $p = 92$ polarization setting because of the onset of Wood's anomaly).

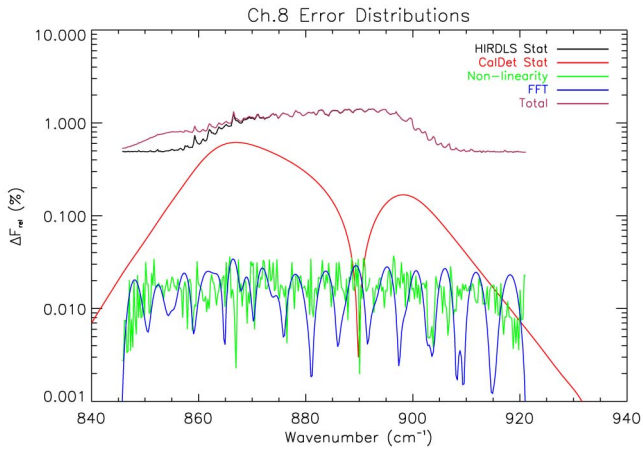

Fig. 13. Statistical and systematic error distributions $\Delta F_{\rm rel}(\overline{\nu})$ (in percent against wavenumber), for channel 8, under nominal instrument operating conditions. The distributions are calculated between the 1% RRPs. Due to its small size, the error distribution belonging to the calibration detector spectral response is not shown (off scale).

TABLE III
WEIGHTED-MEAN ERROR CONTRIBUTIONS FOR THE MEASURED HIRDLS INSTRUMENT SPECTRAL RESPONSES, UNDER NOMINAL INSTRUMENT OPERATING CONDITIONS (I.E., $T_{\rm FPA} \simeq 61$ K AND $T_{\rm Lens1} = 301$ K). DEFINITIONS FOR EACH COLUMN AREA ARE AS FOLLOWS: $\sigma_{1\rm st}$ IS THE HIRDLS STATISTICAL UNCERTAINTY COMPONENT; $\sigma_{2\rm st}$ IS THE MONOCHROMATOR CALIBRATION DETECTOR STATISTICAL UNCERTAINTY COMPONENT; $\sigma_{1\rm sy}$ IS THE SYSTEMATIC ERROR DUE TO THE UNCERTAINTY IN THE RADIOMETRIC NONLINEARITY FACTOR k; $\sigma_{2\rm sy}$ IS THE SYSTEMATIC ERROR DUE TO THE FFT FILTERING CUTOFF WAVELENGTH; $\sigma_{3\rm sy}$ IS THE SYSTEMATIC ERROR DUE TO THE MONOCHROMATOR CALIBRATION DETECTOR SPECTRAL RESPONSE; $\sigma_{\rm tot}$ IS THE QUADRATURE SUM OF THESE ERRORS

Channel Number	σ_{1st} (%)	σ_{2st} (%)	σ_{1sy} (%)	σ_{2sy} (%)	σ_{3sy} (%)	$\sigma_{\rm tot}$ (%)
1	1.457	0.101	0.013	0.119	5.496E-4	1.465
2	0.733	0.093	0.010	0.274	5.848E-4	0.794
3	1.189	0.128	0.013	0.120	1.479E-3	1.202
4	1.425	0.028	0.015	0.248	4.749E-4	1.447
5	1.308	0.064	0.012	0.053	2.219E-3	1.311
6	1.687	0.112	0.009	0.095	8.798E-6	1.693
7	2.266	0.120	0.010	0.758	4.100E-5	2.392
8	1.150	0.285	0.017	0.015	2.290E-5	1.185
9	0.475	0.083	0.007	0.205	8.861E-5	0.524
10	0.760	0.058	0.005	0.057	1.387E-5	0.764
11	0.602	0.092	0.006	0.117	7.970E-5	0.620
12	0.681	0.056	0.005	0.157	5.575E-5	0.701
13	0.969	0.024	0.005	0.129	3.005E-5	0.978
14	0.829	0.026	0.004	0.058	6.633E-5	0.831
15	0.881	0.054	0.011	0.430	6.441E-5	0.982
16	0.536	0.066	0.005	0.221	9.106E-5	0.584
17	1.579	0.193	0.007	0.014	1.706E-4	1.591
18	1.043	0.197	0.009	0.020	2.642E-4	1.062
19	1.631	0.062	0.008	0.325	8.445E-5	1.664
20	1.308	0.333	0.011	0.004	3.776E-4	1.350
21	0.583	0.103	0.006	0.022	6.941E-5	0.592

The error analysis brought out the reality and precision of the hard work that went into this endeavor. The largest contribution to the overall error $\Delta F_{\rm rel}(\overline{\nu})$ for all channels belonged to the HIRDLS spectral response random statistical uncertainty. A highly probable root cause for this outcome could be attributed to the large radiometric signal used for most channels. In general, the larger the signal level through the most spectrally sensitive regions in a channel passband, the larger the standard deviation about the measured mean (see Fig. 1). From an analysis standpoint, using larger signals in some channels was crucial in determining the starting position in HIRDLS time for acquiring the HIRDLS response data, which, in turn, was needed to correctly synchronize the associated external monochromator data set. In particular, when using larger fluxes, the longer wavelength channels experienced larger-than-expected noise levels in the tails, requiring a running boxcar filter applied to the data to help identify the fiducial HIRDLS starting time. To the contrary, shorter wavelength channels, for the most part, had much lower noise levels in the spectral response tails.

A way to circumvent this particular problem would have been to increase the number of measurements N for each polarization setting, thereby weighing the resulting average statistical standard deviation by $N^{-1/2}$. With the short amount of time allocated for the overall calibration period, this statistical fix would have been a highly improbable venture.

The remaining components, both statistical and systematic, making up $\Delta F_{\rm rel}(\overline{\nu})$ are comparatively smaller than the HIRDLS spectral response statistical uncertainty. The error distributions, between the 1% RRPs, for channel 8 under nominal instrument operating conditions are shown in Fig. 13. Table III lists the individual weighted errors, between the 1% RRPs, for all 21 channels, under nominal instrument operating conditions. As an example, the weighted errors for the HIRDLS spectral response statistical error component were calculated using the following relationship:

$$\sigma_{h,v} = \frac{\sum_{i=1}^{N} \Delta F_{\rm rel}^{h,v}(\overline{\nu})_i F_{\rm rel}^{h,v}(\overline{\nu})_i}{\sum_{i=1}^{N} F_{\rm rel}^{h,v}(\overline{\nu})_i}. \tag{16}$$

Here again, h and v represent the polarization settings $p = 36$ and $p = 92$, respectively. Combining each weighted error in quadrature yields the desired result

$$\sigma_{\rm 1st} = \left[(\sigma_h)^2 + (\sigma_v)^2\right]^{1/2}. \tag{17}$$

TABLE IV
WEIGHTED-MEAN ERROR CONTRIBUTIONS FOR THE MEASURED HIRDLS SPECTRAL RESPONSES, UNDER OFF-NOMINAL INSTRUMENT OPERATING CONDITIONS (I.E., $T_{\rm FPA} \simeq 71$ K AND $T_{\rm Lens1} = 301$ K). COLUMN DEFINITIONS ARE IDENTICAL TO THAT IN TABLE III

Channel Number	σ_{1st} (%)	σ_{2st} (%)	σ_{1sy} (%)	σ_{2sy} (%)	σ_{3sy} (%)	$\sigma_{\rm tot}$ (%)
1	1.927	0.095	0.019	0.114	5.218E-4	1.933
2	0.989	0.091	0.015	0.281	5.702E-4	1.032
3	1.353	0.112	0.025	0.132	1.514E-3	1.365
4	1.194	0.028	0.018	0.208	4.707E-4	1.212
5	1.447	0.063	0.012	0.042	2.172E-3	1.449
6	1.009	0.043	0.026	0.109	7.702E-6	1.016
7	0.637	0.102	0.015	0.726	3.946E-5	0.971
8	0.896	0.095	0.014	0.019	2.377E-5	0.901
9	0.548	0.039	0.007	0.242	8.667E-5	0.600
10	0.787	0.340	0.006	0.055	1.248E-5	0.859
11	0.811	0.092	0.011	0.133	7.677E-5	0.827
12	0.642	0.026	0.006	0.184	5.585E-5	0.668
13	1.001	0.029	0.004	0.119	2.856E-5	1.008
14	0.845	0.023	0.005	0.064	6.983E-5	0.847
15	0.727	0.027	0.010	0.419	6.445E-5	0.840
16	0.795	0.025	0.006	0.287	8.837E-5	0.846
17	0.897	0.068	0.010	0.012	1.698E-4	0.900
18	0.533	0.035	0.005	0.030	2.648E-4	0.535
19	1.020	0.011	0.008	0.383	8.816E-5	1.090
20	0.670	0.087	0.006	0.003	3.763E-4	0.676
21	1.132	0.016	0.010	0.021	6.870E-5	1.132

TABLE V
WEIGHTED-MEAN ERROR CONTRIBUTIONS FOR THE MEASURED HIRDLS SPECTRAL RESPONSES, FOR OFF-NOMINAL INSTRUMENT OPERATING CONDITIONS (I.E., $T_{\mathrm{FPA}} \simeq 61$ K AND $T_{\mathrm{Lens1}} = 291$ K). COLUMN DEFINITIONS ARE IDENTICAL TO THAT IN TABLE III

Channel Number	σ_{1st} (%)	σ_{2st} (%)	σ_{1sy} (%)	σ_{2sy} (%)	σ_{3sy} (%)	σ_{tot} (%)
1	1.194	0.103	0.020	0.105	5.534E-4	1.203
2	0.545	0.068	0.014	0.286	5.598E-4	0.619
3	2.175	0.134	0.030	0.091	1.757E-3	2.181
4	0.747	0.029	0.013	0.282	4.791E-4	0.799
5	0.599	0.065	0.011	0.076	2.222E-3	0.607
6	0.762	0.053	0.024	0.112	6.410E-6	0.772
7	0.596	0.092	0.012	0.414	3.834E-5	0.732
8	0.930	0.120	0.030	0.014	2.391E-5	0.938
9	0.438	0.036	0.010	0.194	8.059E-5	0.480
10	0.449	0.081	0.006	0.055	1.320E-5	0.460
11	0.413	0.127	0.008	0.035	8.098E-5	0.434
12	0.406	0.025	0.006	0.430	5.099E-5	0.592
13	0.553	0.020	0.004	0.298	3.030E-5	0.629
14	0.425	0.015	0.005	0.059	6.747E-5	0.429
15	0.485	0.038	0.008	0.388	6.403E-5	0.622
16	0.586	0.043	0.007	0.469	9.020E-5	0.752
17	0.658	0.037	0.007	0.019	1.687E-4	0.659
18	0.514	0.036	0.005	0.038	2.597E-4	0.517
19	0.799	0.011	0.007	0.773	8.108E-5	1.112
20	0.606	0.160	0.006	0.012	3.769E-4	0.627
21	0.585	0.088	0.005	0.022	6.853E-5	0.592

Tables IV and V list the weighted errors for the two off-nominal-instrument-operating-condition spectral response data.

The spectral characterization of the HIRDLS flight instrument was the most difficult and challenging component during the prelaunch calibration exercise. Time constraints kept the amount of testing to nearly a bare minimum. Unanticipated problems that mostly occurred at the beginning of the spectral calibration phase (e.g., heating of monochromator elements, adjusting and modifying the calibration detector and associated electronics due to varying background radiation, etc.), slowed initial progress but were overcome to provide some very high quality data, which has ultimately resulted in a reliable spectral characterization of the HIRDLS flight instrument.

ACKNOWLEDGMENT

The authors would like to thank the many people involved throughout the calibration exercise: University of Oxford personnel (engineers, machinists, scientists, etc.), Lockheed Martin personnel, and many others from the National Center for Atmospheric Research, the University of Colorado at Boulder, and NASA. In particular, special recognition goes out to C. Palmer for his many in-depth and careful contributions early on to the prelaunch calibration program.

REFERENCES

[1] J. Gille, J. Barnett, J. Whitney, M. Dials, D. Woodward, W. Rudolf, A. Lambert, and W. Mankin, "The High Resolution Dynamics Limb Sounder (HIRDLS) experiment on Aura," in *Proc. SPIE Infrared Spaceborne Remote Sens. XI*, 2003, vol. 5152, pp. 162–171.

[2] G. J. Hawkins, R. Hunneman, J. J. Barnett, and J. G. Whitney, "Spectral design and verification of HIRDLS filters and antireflection coatings using an integrated system performance approach," *Proc. SPIE*, vol. 3437, pp. 102–112, 1998.

[3] C. L. Hepplewhite, J. J. Barnett, K. Djotni, J. G. Whitney, J. N. Bracken, R. Wolfenden, F. Row, C. W. P. Palmer, R. E. J. Watkins, R. J. Knight, P. F. Gray, and G. Hammond, "HIRDLS monochromator calibration equipment," in *Proc. SPIE Infrared Spaceborne Remote Sens. XI*, 2003, vol. 5152, pp. 205–213.

[4] T. D. Eden, Jr., J. C. Gille, J. J. Barnett, C. L. Hepplewhite, C. W. P. Palmer, and J. G. Whitney, "HIRDLS proto-flight model radiometric calibration from pre-launch calibration data," in *Proc. SPIE Infrared Spaceborne Remote Sens.*, 2005, vol. 5883, pp. L1–L11.

[5] F. E. James and M. Roos, MINUIT, Geneva, Switzerland: CERN, Program for function minimization and error analysis, No. D506, CERN Program Library.

[6] R. W. Wood, "On a remarkable case of uneven distribution of light in a diffraction grating spectrum," *Philos. Mag.*, vol. 4, pp. 396–408, 1902.

Thomas Eden, Jr. received the B.S. degree in physics and the Ph.D. degree in experimental nuclear physics from Kent State University, Kent, OH.

After doing postdoctoral work in nuclear physics for about five years immediately following graduation, he began pursuing research in atmospheric science. In 2002, he joined the High Resolution Dynamics Limb Sounder (HIRDLS) project with the National Center for Atmospheric Research, Boulder, CO, as a Project Scientist, initially concentrating on the prelaunch calibration of the HIRDLS flight instrument. Subsequent efforts on the project have dealt mainly with current on-orbit problems that have plagued HIRDLS since launch. He is currently a Scientific Coinvestigator on the HIRDLS project.

John Barnett, photograph and biography not available at the time of publication.

John Gille received the B.S. degree from Yale University, New Haven, CT, the M.S. degree from the University of Cambridge, Cambridge, U.K., and the Ph.D. degree from Massachusetts Institute of Technology, Cambridge.

He is the U.S. Principal Investigator (PI) for the High Resolution Dynamics Limb Sounder experiment on the Aura satellite and for the Measurements of Pollution in the Troposphere experiment on Terra. He is a Senior Scientist and the Earth Observing System Manager with the National Center for Atmospheric Research, Boulder, CO. He is also an Adjoint Professor with the University of Colorado, Boulder. He has been a Principal Investigator on two previous satellite experiments. He works to develop satellite instruments to measure the composition of the atmosphere and applies the data to the solution of atmospheric problems.

Karim Djotni, photograph and biography not available at the time of publication.

Chris Hepplewhite, photograph and biography not available at the time of publication.

Olusoji Oduleye, photograph and biography not available at the time of publication.

John Whitney, photograph and biography not available at the time of publication.